MICROBIOTA AND HOST

Microbiota and Host (2025) **3** e240008
https://doi.org/10.1530/MAH-24-0008

Received 14 August 2024
Accepted 6 December 2024
Available online 6 December 2024
Version of Record published 9 January 2025

RESEARCH

Interaction between the human dental microbiome and host gingival model

Maki Sotozono, Ryouhei Takahashi, Takako Ida, Ryoko Nagata, Rui Saito, Niraya Kornsombut, Jutharat Manuschai, Shoji Takenaka and Yuichiro Noiri

Division of Cariology, Operative Dentistry and Endodontics, Faculty of Dentistry & Graduate School of Medical and Dental Sciences, Niigata University, Niigata, Japan

Correspondence should be addressed to M Sotozono: sotozono@dent.niigata-u.ac.jp

Abstract

Objective: Interactions between the dental biofilm and host are important to study infectious oral diseases such as dental caries and periodontitis. Previous studies have reported the reaction of a host gingival model cocultured with bacteria or biofilms. However, these studies only report results of a gingival model, and a biofilm cocultured with a gingival model has never been investigated, although the microbiome of dental biofilms is associated with the maintenance of health and the onset of infectious oral diseases. Therefore, we aimed to investigate the reaction of a gingival model and experimental biofilm. An *in situ* dental biofilm model, which enables biofilm formation in the oral cavity, was used to prepare experimental biofilms.

Methods: The *in situ* biofilm was cocultured with a reconstructed human gingival (RHG) model. We performed 16S rRNA sequence analysis, metagenomic function prediction analysis, total bacterial cell counts using quantitative polymerase chain reaction and confocal laser microscopy observation in addition to gene expression and histological investigation of RHG.

Results: We found a change in *Veillonella* abundance in the *in situ* biofilms cocultured with RHG. Metagenomic function prediction analysis revealed that the activity of certain pathways associated with amino acid production, lactic acid fermentation and the glycolysis system significantly increased in biofilms cocultured with RHG.

Conclusion: The microbiome and functions of dental biofilms can be affected by host gingival tissues. Our findings will contribute to the establishment of a host–biofilm interaction model to understand the pathophysiology of oral infectious diseases.

Keywords: dental biofilm; microbiome; oral microbiome; host–microbiome interaction

Introduction

Dental caries and periodontitis are chronic infectious diseases that affect individuals worldwide (Peres *et al.* 2019). The main cause of these diseases is dental biofilm (DB) formation, which involves the growth of oral bacteria on the tooth surface (Clarke 1924, Asikainen *et al.* 1996). The development and progression of dental caries and periodontitis can be affected by many bacterial species: not only specific bacteria but also the entire biofilm composition. An imbalanced composition of the oral microbiome (dysbiosis) contributes to these oral diseases (Hajishengallis & Lamont 2012, Simón-Soro & Mira 2015). DB and host immune responses together contribute to initiation and progression of periodontal disease (Graves 2008, Kinane *et al.* 2017). The aforementioned dysbiosis can play important roles, and the interaction between the microbiome of DBs and the host immune system is associated with periodontal disease development (Abdulkareem *et al.* 2023). Therefore, DBs and their

Published by Bioscientifica Ltd.
https://mah.bioscientifica.com

Microbiota and Host (2025) **3** e240008
https://doi.org/10.1530/MAH-24-0008

dysbiosis are associated with oral infectious diseases. The control and reduction of DB formation are considered an important approach for the prevention of oral diseases, such as dental caries and periodontitis. Although bacteria can cause various infectious diseases in the host, commensal bacteria can positively affect host health. In the gastrointestinal tract inhabited by commensal bacteria, the host tissue secretes cytokines and chemical mediators against commensal bacteria and their metabolic products and it regulates the immune system and functions (Brestoff & Artis 2013). In the oral cavity and gastrointestinal tract, DBs can help the host maintain the homeostasis and functions of the gingival epithelium, and the imbalance between the host immune system and dysbiotic DB can lead to the development of oral infectious diseases such as periodontitis (Shang *et al.* 2018). The interaction between DBs and the host can be considered important to understand the development of oral infectious diseases.

To investigate the interaction between the host and DBs, many studies utilized a host–biofilm coculturing system. In these studies, investigating the interaction in the oral cavity of the host involves studying the gingival tissue, which is in contact with the DB. In the host gingival model, human gingival cell lines and a reconstructed human gingival (RHG) model, which is cultured using gingival epithelial and fibroblast cell lines, are used because human gingival tissues cannot be used owing to ethical concerns.

Various biofilms are used for exposure to host models, such as the RHG model. In a previous study, a single-species biofilm comprising *Porphyromonas gingivalis* and a multispecies biofilm comprising several bacterial species were used. However, because more than 700 bacterial species inhabit the oral cavity (Kroes *et al.* 1999, Aas *et al.* 2005), the use of single- and multispecies *in vitro* biofilms is insufficient to investigate the host–DB interaction. To use bacteria living in the oral cavity, saliva has been collected and cultured *in vitro* for the formation of an experimental DB, and the experimental biofilm cultured in this method is often called a saliva-derived biofilm. The Human Microbiome Project (2007–2017) revealed the compositions and characteristics of the microbiomes in various parts of the body (Human Microbiome Project Consortium 2012*a*). In this project, the oral cavity showed high microbial diversity in the human body and parts of the oral cavity. It was reported that the microbiome of the saliva differs from that of DBs (Human Microbiome Project Consortium 2012*b*, Sotozono *et al.* 2021*a*), and there remains a problem of using saliva-derived biofilms as an experimental biofilm. Moreover, the behavior of biofilms has not been investigated, although the reactions of the RHG model have been investigated in these previous studies.

In the present study, an *in situ* DB model, which enables the formation of an experimental biofilm in the oral cavity, was used (Wake *et al.* 2016). This model consisted of oral appliances and hydroxyapatite (HA) disks inserted to the buccal side of the appliances. The experimental biofilm attaches onto the HA disks, which can be collected as biofilm samples without destroying the three-dimensional structures. Moreover, biofilm samples prepared using this model have a microbiome that resembles that of DBs growing on the tooth surface. Based on the limitations of experimental biofilms in previous studies and insufficient analysis of biofilms, the purpose of this study is to analyze both the RHG and experimental biofilm formed using the *in situ* DB model. We hypothesize that the *in situ* DB can be affected by the host gingiva model.

Materials and methods

Subjects

Ten subjects, including six men and four women (age 25–32 years), were recruited from the staff and students of the Niigata University Graduate School of Medical and Dental Sciences, Niigata, Japan. Healthy subjects were defined as described previously (Aagaard *et al.* 2013). The exclusion criteria are as follows: systemic disease, dental caries, periodontitis, use of antibacterial agents within 3 months, use of mouthwash containing bactericidal ingredients within 2 weeks and smoking. The characteristics of the subjects are presented in Table S1 (see the section on Supplementary materials given at the end of the article).

Subject consent and ethical declarations

The subjects received a detailed explanation of the objectives and methods of this study. The subjects were also informed about the confidentiality of the information collected during the experiment. Written informed consent forms were obtained from all subjects. The study design was approved by the Ethics Committee of Niigata University (Approval Number: 2021-0041). This study was conducted in accordance with the Ethical Guidelines for Medical and Biological Research Involving Human Subjects. The experiments were conducted in accordance with the guidelines of the Declaration of Helsinki.

DB sample formation and sampling

DB sample formation was performed using the *in situ* DB model as previously described (Wake *et al.* 2016, Sotozono *et al.* 2021*b*). Oral appliances for the *in situ* DB model were prepared using an ethylene vinyl acetate sheet (SHOFU, Japan). HA disks (Olympus Terumo Biomaterials, Japan) were buccally inserted onto the bilateral first premolars, second premolars, first molars and second molars (Fig. 1A).

Microbiota and Host (2025) **3** e240008
https://doi.org/10.1530/MAH-24-0008

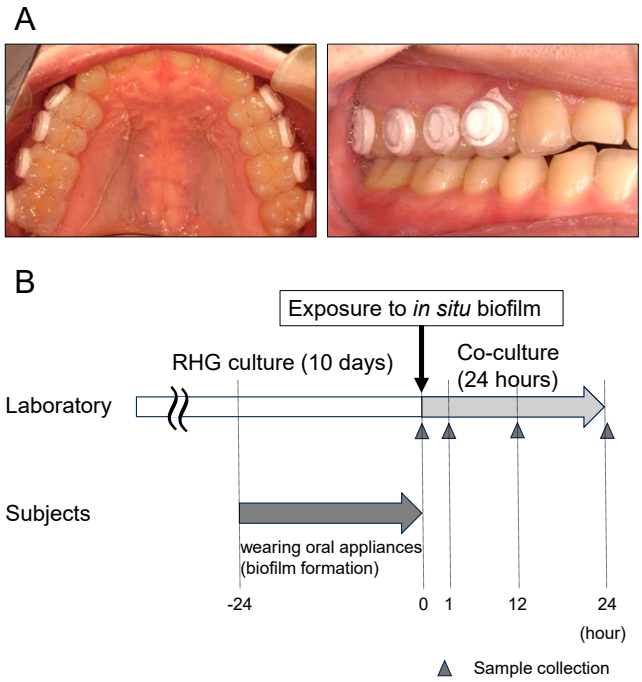

Figure 1

In situ dental biofilm model and experimental schedule. (A) The pictures of the *in situ* dental model are shown. The oral appliances are set on the upper jaw of a subject. Eight hydroxyapatite disks are inserted on the buccal surface of the oral appliance. (B) The experimental schedule is shown. In the laboratory, RHG was cultured 10 days before exposure to the *in situ* DB. Subjects started wearing the oral appliances 24 h before the *in situ* DB was exposed to RHG.

The oral appliance was sterilized using ethylene oxide gas before the experiment.

The subjects wore the oral appliance after brushing their teeth. During meals and brushing, the device was removed and kept in a Petri dish coated with saline solution to prevent drying. The subjects brushed their teeth after eating and then resumed wearing the oral appliance. Toothpaste was not used during brushing. While wearing the oral appliance, fluid intake was limited to water. Biofilm samples on HA disks were collected after the subjects had worn the oral appliance for 24 h. The biofilms on the HA disks were used as DB samples.

Cell culture

Immortalized human gingival fibroblasts (hGFBs; ATCC-4061; ATCC, USA) were cultured in Dulbecco's modified Eagle medium (DMEM, Thermo Fisher Scientific, USA) supplemented with 10% fetal bovine serum at 37 °C with 5% CO_2 and 95% humidity until 80–90% confluence. Immortalized human gingival epithelial cells (hTERT TIGKs; ATCC-3397, ATCC) were cultured in dermal cell basal medium (ATCC) supplemented with a keratinocyte growth kit (PCS-200-040; ATCC) until 80–90% confluence was attained before constructing the RHG model.

RHG culture

RHG was cultured using a slightly modified version of a previously used protocol (Buskermolen *et al.* 2016, Holm & Qu 2022). A collagen mixture was prepared by sequentially mixing 0.3% cell matrix type IA, 5× DMEM and reconstitution buffer (Nitta Gelatin, Japan) according to the product description. hGFBs (1×10^5 cells/mL) were added to the prepared collagen gel matrix. Subsequently, 400 μL hGFB-populated collagen mixture were pipetted into a 0.4 μm pore size Transwell insert (Corning, USA). Cultured hTERT TIGKs (4.5×10^5 cells/mL) were added to the keratinocyte growth medium according to a previous study (Shang *et al.* 2018). Concentration-adjusted hTERT TIGKs were added to the top of the hGFB-populated collagen gel (500 μL per insert). Subsequently, 2 mL keratinocyte growth medium were added per well and hTERT TIGKs were incubated in solution for 3 days. The keratinocyte growth medium was aspirated and transferred to an air–liquid interface culture for 7 days.

Coculture of DB sample and RHG

After incubation for 10 days, the HA disks on which the DBs adhere to and the RHG cultures were cocultured as previously described (Brown *et al.* 2019, Redanz *et al.* 2021). First, a 0.5 mm thick silicone loop was placed on the RHG. The HA disk was then placed on top of that silicone loop with the formed DB facing the RHG. The space between the RHG and HA disk was filled with saline solution. Samples of the HA disk and RHG were collected before coculture at baseline and at 1, 12 and 24 h after the start of coculture. In this study, it was necessary to prepare two kinds of 'controls' for coculturing experiments to investigate two samples: DBs (biofilm) and RHG (host). One control involved a DB sample cocultured with the collagen gel without fibroblasts and keratinocytes for DB investigation. The other control involved an RHG sample cocultured with a sterilized HA disk without experimental biofilms for RHG investigation. Therefore, four sample types were obtained: an RHG sample cocultured with a DB sample, a DB sample cocultured with an RHG sample, a control DB sample cocultured with only the collagen gel (control for DB investigation) and a control RHG sample cocultured with a sterilized HA disk (control for RHG investigation).

Experimental protocol

DB samples were collected before coculture at baseline and at 1, 12 and 24 h after coculture. RHG samples were collected at 1, 12 and 24 h after coculture. The experimental schedule is shown in Fig. 1B. Because the number of biofilm samples prepared using the *in situ* DB model is limited to eight at a single time,

Microbiota and Host (2025) **3** e240008
https://doi.org/10.1530/MAH-24-0008

the experiments were performed separately in two phases. In the first phase, total bacterial count analysis using quantitative polymerase chain reaction (qPCR) and 16S ribosomal RNA amplicon sequence analysis were performed after the extraction of bacterial DNA from DB samples. RNA extracted from RHG samples was used for reverse transcription-qPCR for the investigation of gene expression. In the second phase, DB samples were observed using confocal laser scanning microscopy (CLSM). RHG samples were used for histological observation.

Total bacterial count determined via qPCR

HA disks collected were used for DNA extraction. Bacterial DNA was extracted using a DNeasy® PowerSoil® Pro Kit (QIAGEN, Germany) following the manufacturer's instructions. HA disks on which biofilm samples attached to were put into sample tubes in a DNA extraction kit, and HA disks and biofilm samples in sample tubes were shaken with beads for crushing bacteria. The number of total bacteria was determined using qPCR on a StepOne™ real-time PCR system (Thermo Fisher Scientific). A Power SYBR® Green Master Mix (Applied Biosystems, USA) and universal primers specific to the 16S ribosomal RNA gene hypervariable region V1–V2 were used and the concentration was 500 nM (Wake *et al.* 2016, Sotozono *et al.* 2021*b*). The universal primer sequences are presented in Table S2. The standard curve for determining bacterial counts using qPCR was constructed using *Streptococcus mutans* ATCC 25175 DNA.

16S ribosomal RNA amplicon sequence analysis

The V1–V2 region was amplified, and the PCR amplicon libraries were quantified using a Synergy H1 (Agilent Technologies, USA) and a QuantiFluor dsDNA system. Library quality was assessed using a fragment analyzer and a dsDNA 915 Reagent Kit (Agilent Technologies). DNA sequencing was performed using Miseq Reagent Kit v3 (Agilent Technologies) and Illumina Miseq® using 300 bp paired-end reads. Phylogenetic inference was conducted using the feature-classifier plugin by comparing the obtained representative sequences with the 16S ribosomal RNA operational taxonomic units clustered at a 97% identity threshold in the Greengenes database version 13_8 for the 16S rRNA region spanning the V1–V2 region. Metagenomic function prediction analysis was performed with the use of the PICRUST2 pipeline in Qiime2 based on the sequences obtained above.

CLSM observation

DB samples were washed with PBS. We used a modified version of a biofilm staining method used previously (Wake *et al.* 2016, Sotozono *et al.* 2021*b*). DB samples stained using a LIVE/DEAD® BacLight™ Bacterial Viability Kit (BacLight staining; Invitrogen, USA), CF®405-labeled lectin concanavalin A (Con A; Biotium, USA) and wheat germ agglutinin (WGA; Biotium) were observed using CLSM (LSM 700; Carl Zeiss, Germany). Three locations per sample were randomly recorded. Image processing was performed using Imaris® software version 9.6.0. (Bitplane AG, Switzerland; https://imaris.oxinst.com/products/image-analysis-software/) to reconstruct three-dimensional images and calculate the volumes of viable bacterial cells, dead bacterial cells and exopolysaccharides (EPSs).

Gene expression analysis via reverse transcription-qPCR

RNA was extracted from RHG samples using an RNeasy® Mini Kit (QIAGEN) following the manufacturer's instructions. MagNA Lyser (Roche Diagnostics K.K., Japan) was used for crushing the RHG samples. Reverse transcription to yield cDNA was performed using the High-Capacity cDNA Reverse Transcription Kit (Applied Biosystems, Foster City, CA, USA). qPCR was subsequently performed on a StepOne™ real-time PCR system using primers for human cathelicidin (LL-37), human beta defensin (hBD-1, *DEFB1*; hBD-2, *DEFB2*; hBD-3 and *DEFB3*), adrenomedullin (*ADM*), interleukin-6 (*IL6*), *IL1B*, tumor necrosis factor-alpha (*TNF*), *IL8* and glyceraldehyde 3-phosphate dehydrogenase (*GAPDH*). The sequences of primers and the references are shown in Table S2 (Weisburg *et al.* 1991,.Suzuki & Giovannoni 1996, Chandra *et al.* 2011, Bogefors *et al.* 2012, Wolgin *et al.* 2012, Filho *et al.* 2015, Pahumunto *et al.* 2017, Zhang *et al.* 2021). Gene expression was normalized to that of the housekeeping gene *GAPDH* using the $2^{-\Delta\Delta CT}$ method. The internal control gene *GAPDH* was used to determine the relative abundance and cycle threshold range of the gene.

Cell viability assay

A cell viability assay using cell counting kit-8 (DOJINDO LABORATORIES, Japan) was performed following the manufacturer's instructions. Briefly, RHG samples were treated with collagenase (FUJIFILM Wako Pure Chemical Corporation, Japan) for 1 h at 37 °C and resuspended in DMEM before adding the cell counting kit-8. The cell suspension was incubated at 37 °C for 1 h and the absorbance was measured at 450 nm using a GloMax microplate reader (Promega, USA). DMEM was used as a negative control.

Histological evaluation

Tissue sections of the RHG model were stained and observed under a microscope. RHG samples were

Microbiota and Host (2025) **3** e240008
https://doi.org/10.1530/MAH-24-0008

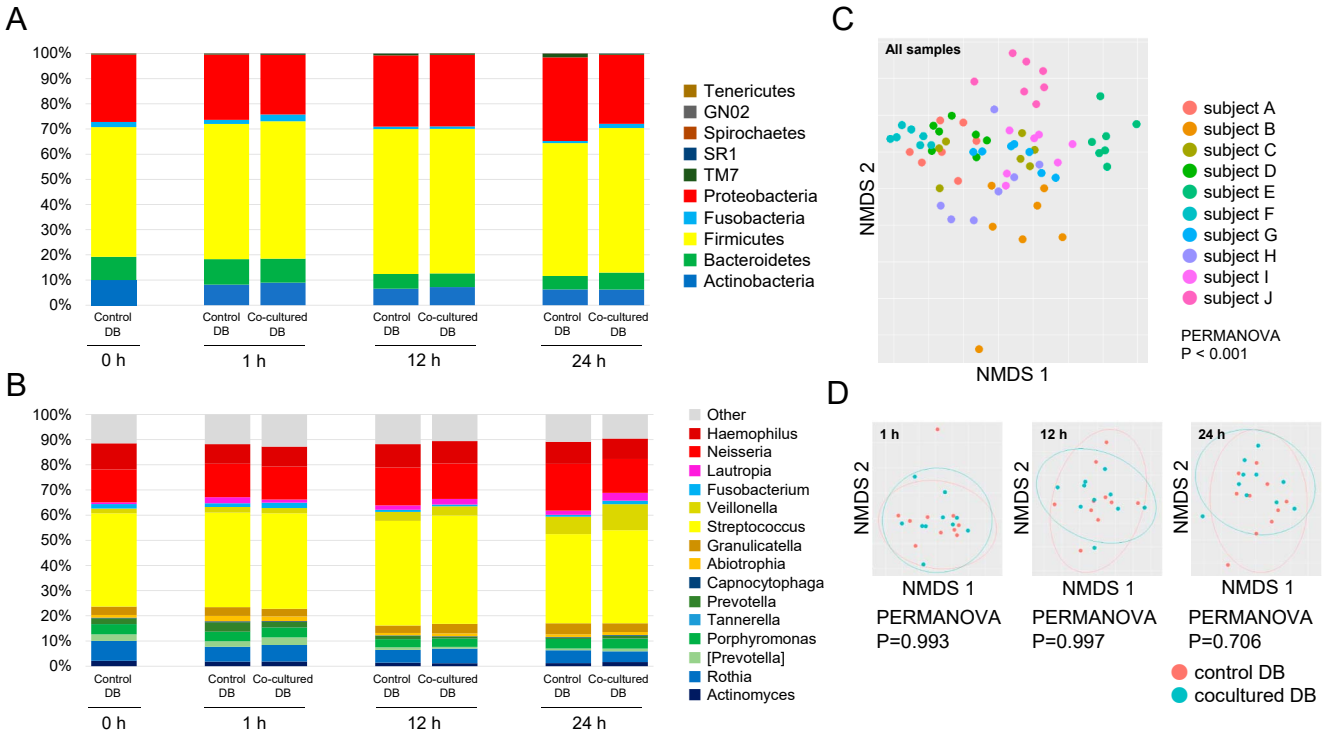

Figure 2

Relative abundance of bacterial taxa and NMDS plots. (A) The relative abundance of bacteria in the DB cocultured with and without RHG at the phylum level. The colors of bars indicate bacterial taxa. (B) The relative abundance of bacteria in the DB cocultured with and without RHG at the genus level. The colors of bars indicate bacterial taxa. (C) Nonmetric multidimensional scaling and permutational multivariate analysis of variance (PERMANOVA) based on the Bray–Curtis distance were performed to compare the microbial profiles of the DB cocultured with (cocultured DB) and without (control DB) RHG. The colors of plots indicate subjects. (D) Microbial profiles are compared between the control DB and cocultured DB by PERMANOVA. The colors of plots indicate the existence of coculturing with RHG. The ellipses in plot area are probability ellipses.

prepared as described previously (Baldeon-Gutierrez *et al.* 2024), with modifications.

Statistical analysis

All data from the experiments were analyzed using IBM SPSS® Statistics (version 22.0, IBM SPSS, USA) and R v4.3.1 (R Core Team, Austria; https://www.r-project.org/). One-way analysis of variance and Tukey test were used for cell viability assay. Friedman's test was used to compare the number of total bacteria and the volumes of live bacteria, dead bacteria and EPS. The Wilcoxon signed-rank test was used to compare relative proportions at the phylum and genus levels in the DB and gene expression in RHG samples. Beta diversity was assessed using the Bray–Curtis distance, and the results were visualized using nonmetric multidimensional scaling (NMDS) plots. The permutational multivariate analysis of variance (PERMANOVA) test was used to detect differences of profiles (Sotozono *et al.* 2021*a*). Spearman's rank correlation coefficient was calculated using SPSS software (https://www.ibm.com/products/spss-statistics). Differences among groups with a *P*-value of <0.05 were considered significant.

Results

Total bacterial count via qPCR

The total bacterial count tended to increase over time; however, a significant difference was not observed between the counts of the control DB group and coculture DB group (Fig. S1).

16S ribosomal RNA amplicon sequence analysis

At the phylum level, five phyla, including Actinobacteria, Bacteroidetes, Firmicutes, Fusobacteria and Proteobacteria, comprised a large portion of the DB microbiome cocultured with and without RHG (Fig. 2A). The relative abundance of Actinobacteria was almost unchanged during the experimental period; however, the abundance of Bacteroidetes reduced at 12 and 24 h in both the control DB and cocultured DB groups. More than 50% of biofilm-forming bacteria in the control DB and cocultured DB groups belonged to Firmicutes. At the genus level (Fig. 2B), the relative abundance of *Veillonella* increased over time and that in the cocultured

DB group was higher than that in the control DB group at 24 h (Wilcoxon signed-rank test, $P = 0.047$).

NMDS based on the Bray–Curtis distance and PERMANOVA were performed to investigate the diversity of the DB microbiome cocultured with and without RHG (Fig. 2C and D). The microbiomes of all samples could be significantly separated based on individual subjects (Fig. 2C, PERMANOVA: $P < 0.001$). However, no significant difference was observed in microbiomes between the control DB and cocultured DB at 1, 12 and 24 h (Fig. 2D).

In addition to the analysis of the microbiome composition, metagenomic function prediction analysis was performed using the PICRUSt2 command pipeline because it is difficult to evaluate the characteristics of the DB based on the results of the microbiome composition alone. The structures of pathway patterns were compared using principal component analysis (PCA). The PCA plots are shown in Fig. 3A and B. Significant interindividual differences were detected in structures of the DB function using PERMANOVA (Fig. 3A, PERMANOVA: $P < 0.001$), although there was no significant difference between functions of the control DB and cocultured DB at 1, 12 and 24 h (Fig. 3B, PERMANOVA, 1 h: $P = 0.926$, 12 h: $P = 0.888$ and 24 h: $P = 0.748$). Some pathways were significantly upregulated in the cocultured DB compared with that in the control DB. Pathways with significant differences in activity between the two groups at each time point are shown in Fig. 3C and D. The pathways associated with amino acid production, lactic acid fermentation and the glycolysis system were more upregulated in the cocultured DB than in the control DB at 1 h. At 24 h, the pathways associated with acetylglucosamine synthesis/degradation and tyrosine synthesis were upregulated significantly in the cocultured DB. Moreover, the activities of glycolysis, coenzyme synthesis, methionine synthesis and folic acid production pathways in the cocultured DB were higher than those in the control DB.

CLSM observation

The microcolonies and fusing colonies developed during the experimental period are shown in Fig. 4A. The volume of dead bacteria in the control DB was higher than that of the cocultured DB at 1 h and that of the co-cultured DB increased significantly over time from 1 to 12 h (Fig. 4D). There was no significant difference in the volume of live bacteria and EPS during the experimental period (Fig. 4B and C). In this study, dead bacteria were surrounded by live bacteria in the CLSM image regardless of time points and with or without coculture.

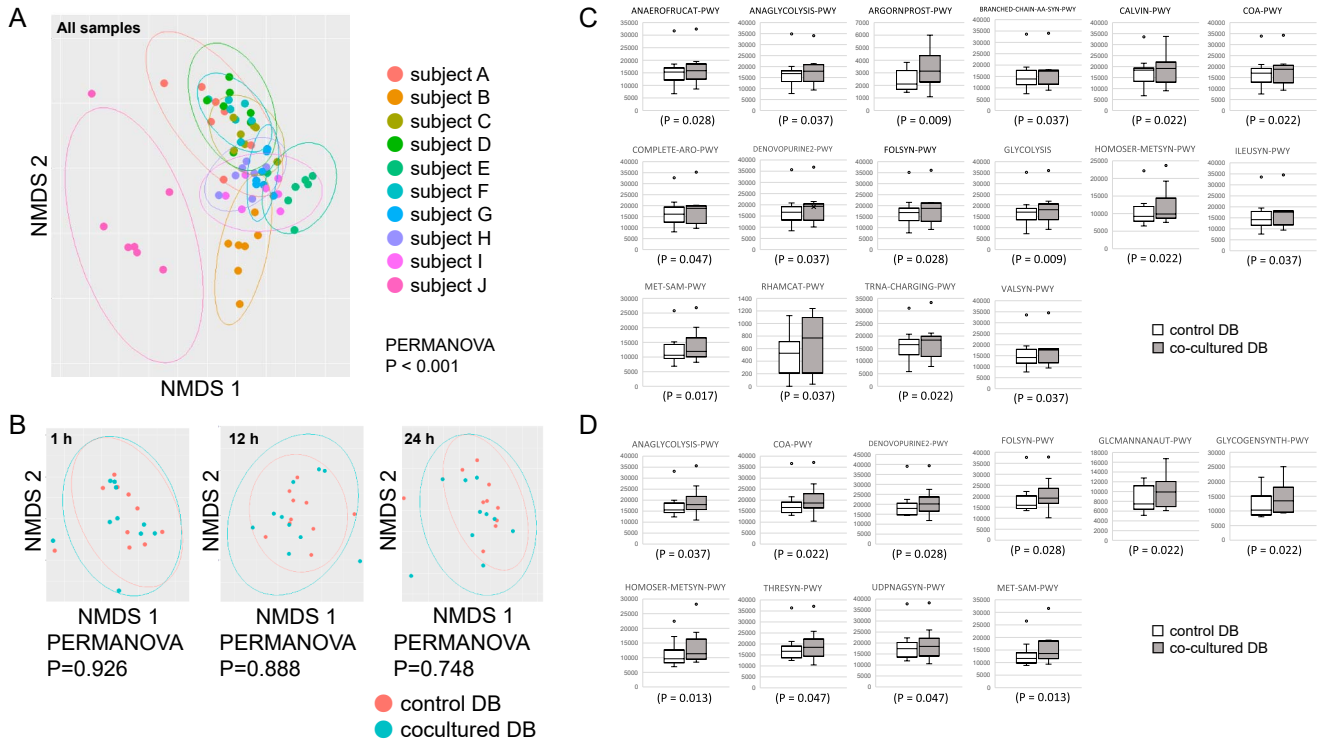

Figure 3

Metagenomic function predicted from the 16S rRNA sequence. (A) Profiles of the predicted function in DB samples of all subjects were compared by PERMANOVA. The colors of plots indicate subjects and the ellipses in plot area are probability ellipses. (B) Profiles of the predicted function in DB samples at each sample collection time were compared by PERMANOVA. The colors of plots indicate existence of coculturing with RHG. The ellipses in plot area are probability ellipses. (C) and (D) Pathways for which significant differences between control and co-cultured DB at 1 h (C) and 24 h (D) are shown (Wilcoxon signed rank test, $P < 0.05$). *Y*-axis denotes the numbers of reads associated with the pathway. Circles indicates outliers. Numbers in parentheses indicate the *P*-value determined by Wilcoxon signed-rank test.

Microbiota and Host (2025) **3** e240008
https://doi.org/10.1530/MAH-24-0008

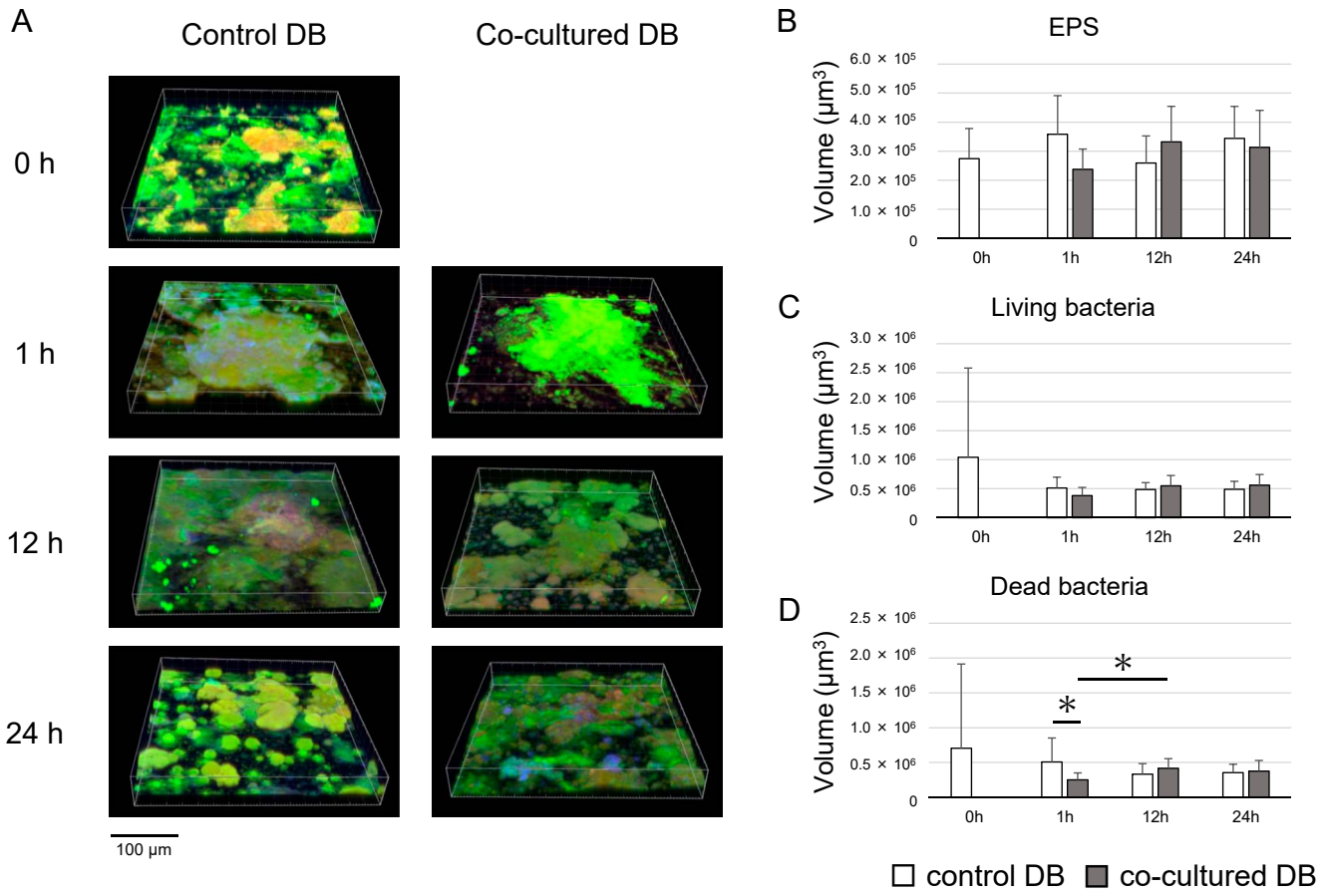

Figure 4

Confocal laser scanning microscopy (CLSM) images and the volumes of EPS, living bacteria and dead bacteria. (A) Representative images of CLSM observation are shown at each sample collection time. EPS labeled with CF-405 Con A and WGA is blue. Living bacteria are depicted in green and dead bacteria are depicted in red with LIVE/DEAD® BacLight™ Bacterial Viability Kit. (B), (C), (D) The volumes of EPS (B), living bacteria (C) and dead bacteria (D) are calculated using Imaris software. Asterisk means significant difference (Friedman test, $P < 0.05$).

Gene expression analysis via reverse transcription-qPCR

The relative gene expression level of *IL8* tended to be lower in the cocultured RHG group than in the control RHG group during the experimental period, and a significant difference was observed at 24 h (Fig. 5A, Wilcoxon signed-rank test, $P = 0.013$). The relative gene expression level of *TNF* tended to decrease over time in the cocultured RHG group, although a significant difference was not observed. In contrast to *TNF*, *IL1B* expression increased over time and it was higher in the cocultured RHG group than in the control RHG group at 12 and 24 h (Wilcoxon signed-rank test, 12 h: $P = 0.022$, 24 h: $P = 0.028$). There was no significant difference in *IL6* expression, although the relative expression was higher at 1 and 12 h and was lower in cocultured RHG than in control RHG. The relative gene expression level of *hBD-1* and *LL-37* was significantly higher at 24 h in cocultured RHG than in control RHG (Fig. 5B, Wilcoxon signed-rank test, *hBD-1*: $P = 0.022$, *LL-37*: $P = 0.017$).

Cell viability assay

The result of the cell viability assay is shown in Fig. S2. The viability of cocultured RHG did not change significantly compared with that of control RHG.

Histological evaluation

Although no histological changes were observed over time in the same group, the increase in the thickness of the keratinocyte layer was observed at all sample collection times in the cocultured RHG group compared with that in the control RHG group. The increase in thickness was observed in all RHG samples cocultured with the DB collected from the ten subjects, although the extents of the increase differed among the subjects (Fig. 5C).

Microbiota and Host (2025) **3** e240008
https://doi.org/10.1530/MAH-24-0008

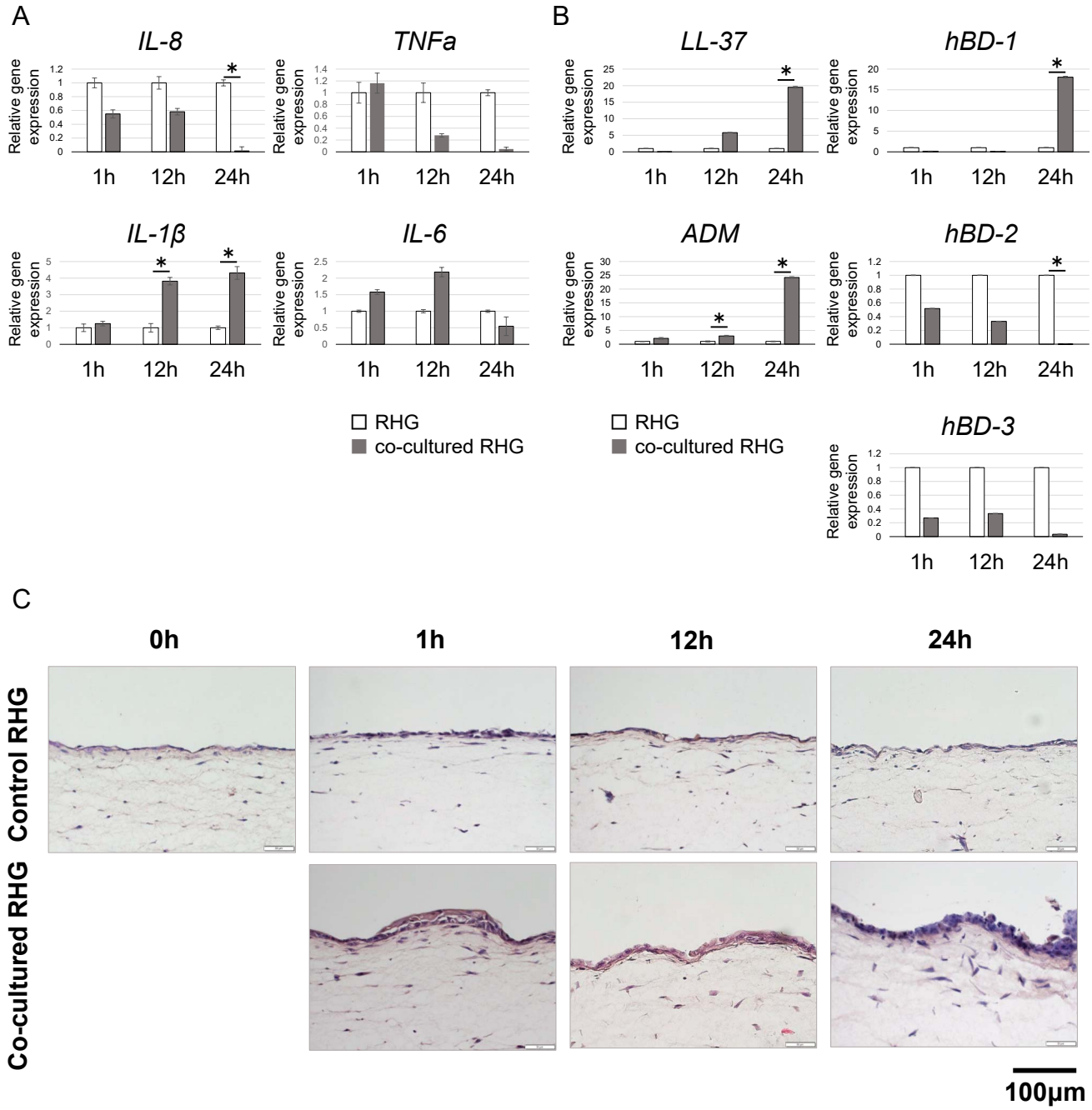

Figure 5

Gene expressions in RHG and histological image of RHG. Gene expressions of inflammatory cytokines (A) and antibacterial peptides (B) in RHG was quantified by real-time PCR. The significance was tested compared with the control RHG of each time point. Asterisk means significant difference (Wilcoxon rank-signed test, $P < 0.05$). The increase in the thickness of the keratinocyte layer was observed at all sample collection times in the cocultured RHG group compared with the control RHG group. The increase in thickness was observed in all RHG samples cocultured with the DB (C).

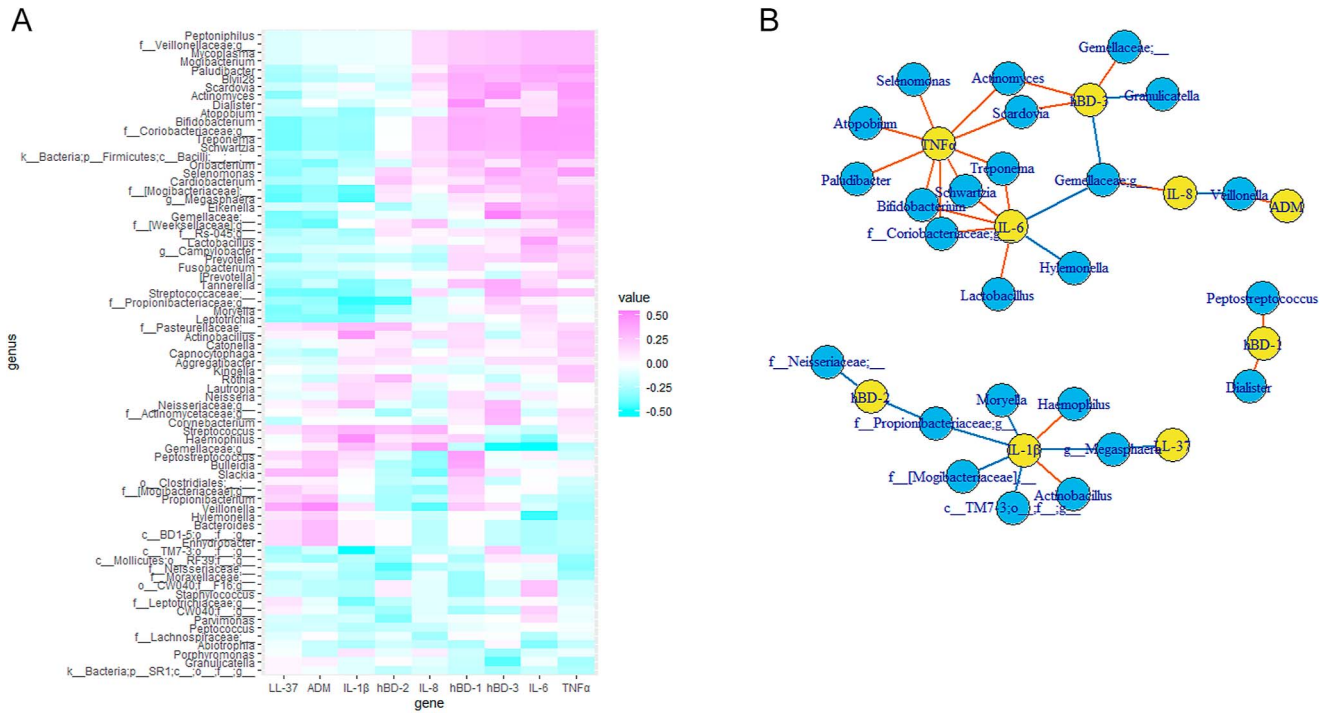

Figure 6

The relationship between the gene expression of RHG and the microbiome Spearman's rank correlation coefficient was calculated based on two parameters: gene expressions in RHG and the bacterial taxa of the microbiome in the DB. The whole results are shown in the heatmap (A) and significant relationships were plotted in the network map (B, Spearman's rank correlation coefficient, $P < 0.05$). In the network map, yellow nodes indicate genes and blue nodes indicate bacterial taxa. Orange edges mean a positive relationship and blue edges mean a negative relationship.

Relation between DB and RHG samples

TNF-α showed positive correlations with some taxa, such as *Actinomyces*, *Treponema* and *Bifidobacterium*. TNF-α and IL-6 showed positive correlations with few of the same taxa: *Treponema*, *Bifidobacterium* and *Schiwartzia*. Moreover, hBD-3 showed a corelationship with *Actinomyces* and *Scardovia*, which were associated with TNF-α. *Veillonella* had a positive correlation with ADM and a negative correlation with IL-8 (Fig. 6).

Discussion

The aim of this study was to investigate the interaction between an experimental DB and a host gingival model. Previous studies have reported an increase in gene expression of antibacterial peptides and cytokines as a host response in a gingival model exposed to a biofilm. However, no studies have investigated the response of a biofilm exposed to gingiva and the relationship between the biofilm and the hosts. Our study reports the first investigation of the response of a DB to a host gingival model. Moreover, the *in situ* DB model applied for biofilm formation in this study has an important advantage that enables us to collect experimental biofilms, in which the microbiome construction is similar to that in DBs formed on the tooth surface in the oral cavity, without destroying the structure. DB samples prepared by using the *in situ* DB model contain cells from buccal mucosa. Buccal mucosal cells in DB samples can affect RHG, when DB samples and RHG are cocultured. However, it is difficult to isolate mucosal cells from DB samples without disturbing the structure of the DB sample. Therefore, we used an HA disk of whose surface the biofilm attached to, as 'DB samples' in this study. In further studies, it is important to investigate the effects of mucosal cells in DB samples.

qPCR using 16S rRNA universal primers revealed that the number of biofilm-forming bacteria increased over time, although no significant differences were observed between the two groups and during the experimental period. Oral bacteria collected using the *in situ* DB model can grow and form colonies on agar plates under aerobic conditions, although not all bacterial species can grow under these conditions (Wake *et al.* 2016, Sotozono *et al.* 2021*b*). The increase in the number of total bacteria under the cell culture conditions may be because of the time course of this study.

Microbiomes obtained from the same research subjects were clustered using PERMANOVA. This result was consistent with that of a previous study that investigated the interpersonal and intrapersonal

Microbiota and Host (2025) **3** e240008
https://doi.org/10.1530/MAH-24-0008

differences in the microbiomes of DBs (Hall *et al.* 2017). At the genus level, a significant difference in the relative abundance of *Veillonella* was observed at 24 h between the control DB group and cocultured DB group. *Veillonella* is considered an early colonizer in the process of DB formation (Simon-Soro *et al.* 2022), and this genus contains nitrate-reducing bacteria that can promote host homeostasis and oral health (Lundberg *et al.* 2009, L'Heureux *et al.* 2023). In contrast, *Veillonella* has been reported to be associated with colony formation of late colonizers such as *P. gingivalis*, *Fusobacterium nucleatum* and *Aggregatibacter actinomycetemcomitans* that are known periodontal pathogens (Periasamy & Kolenbrander 2009, Periasamy & Kolenbrander 2010). It is difficult to estimate and investigate the characteristics of DBs based on the relative abundance at the genus level. Therefore, metagenomic function prediction analysis was performed using PICRUSt2. The analysis revealed that certain pathways were upregulated in the DB cocultured with RHG. The experimental system of this study protocol was a closed system in which the nutrient source is limited. The medium for the RHG culture and the metabolites derived from RHG and the DB could have served as a nutrient source for the DB cocultured with RHG. In contrast, the medium for RHG and the metabolites of the DB alone served as a nutrient source for the DB cultured without RHG. The increase in activity of various pathways in the DB cocultured with RHG suggests that bacteria in DBs use metabolites from RHG as nutrients in this closed system. A previous study using an animal model reported that *Enterococcus coli,* a commensal bacterium in the intestines, can prevent the colonization of *Salmonella*, a pathogenic bacterium associated with intestinal inflammation, by competing for nitrate derived from host intestinal cells (Liou *et al.* 2022). Oral infectious diseases such as dental caries and periodontitis exhibit certain aspects different from those of other systemic infectious diseases, and it is unclear whether the human body possesses preventive mechanisms involving competition of commensal bacteria with pathogens for metabolites derived from the host gingival tissue. However, elucidating the nutrient supply from the host to the DB is important to understand the interaction of DBs and host gingiva.

Microscopic analysis revealed the three-dimensional structure of the DB samples. The *in situ* DB model greatly contributed to this analysis as it allows the collection of the experimental DB formed in oral cavities of research subjects without disturbing the structure of the experimental DB. The *in situ* DB developing in the oral cavity shows a similar structure in which dead bacterial cells are observed at the bottom and live bacterial cells are present at the surface; the volume of dead cells at the bottom of the biofilm tended to increase as the volume of live bacteria increased (Wake *et al.* 2016). This may be attributed to a better nutrient condition at the top of the biofilm than that at the bottom (Yao *et al.* 2022). Immediately after starting the coculture of the DB and RHG, the nutrient condition was better in the control DB than that in the cocultured DB because nutrients are shared with RHG in the cocultured DB and the metabolites from RHG are not enough. This may explain the lower volumes of live and dead bacteria in the cocultured DB than in the control DB and the low volume of dead bacteria at 1 h in this study. However, the culture condition in this study was not all bacterial species in DB samples because DB samples contained obligate anaerobes. It is difficult and impossible to establish the condition suitable for both aerobic and anaerobic bacteria. The dead bacteria detected in the CLSM observation may contain much obligate anaerobes, although in this study, dead bacteria could not be identified. This is one of the limitations of this study.

Shang and coworkers reported that hBD-2 and hBD-3 expression significantly differ compared with those in the control group; the expression of hBD1, LL-37 and ADM does not differ, which contradicts the results of this study (Shang *et al.* 2018). hBD-1 is expressed continuously in epithelial tissues and is called a 'restless warrior' (Prado-Montes de Oca 2010). In contrast, hBD-2 expression is induced by inflammatory cytokines such as TNF-α (Harder *et al.* 2000) and IL-1β (Bals *et al.* 1998), and hBD-3 is induced by TNF-a (Harder *et al.* 2001). Spearman's rank correlation coefficient revealed that *DEFB2* expression had a significant positive corelationship with *TNF* expression and a positive corelationship with *IL1B* expression, which was not significant. The corelationship between the gene expression of *TNF* and *DEFB3* was positive but not significant (Table S3). These results are in agreement with previous findings on the induction of hBD-2 and hBD-3 by TNF-α and IL-1β. The gene expression of inflammatory cytokines is dependent on the cell lines exposed to *in vitro* single-species and multispecies biofilms (Redanz *et al.* 2021). One of the reasons why our results of gene expression did not match those of a previous study may be because of the difference in cell lines used for the RHG model and the differing expression of inflammatory cytokines that can alter the gene expression pattern of antibacterial peptides. Moreover, the gene expression pattern of not only antibacterial peptides but also of inflammatory cytokines differed from that reported previously by Redanz and coworkers. Another reason may involve the microbiome construction of experimental biofilms. Gene expression in RHG is considered to depend on both cell lines and bacterial species (Redanz *et al.* 2021). However, it is difficult to discuss the interaction between DBs and the host model from the perspective of only gene expression in the host model when comparing with previous studies because previous studies did not investigate the microbiome of saliva-derived multispecies biofilms. Therefore, the analysis of the relationship between the DB microbiome and the

gene expression in RHG was performed in the present study. Although many studies have investigated host reaction upon exposure to bacteria and biofilms, this study is the first to investigate the interaction between the host gingival model and the experimental DB via analysis of the host gingival model and the DB microbiome.

The keratinocyte layer of the RHG model was thinner than that reported previously (Shang *et al.* 2018) because the RHG model in this study mimics the epithelium of the gingival sulcus, which faces the DB on the tooth surface. In this study, the cell viability assay revealed the viability of cells in RHG was not affected by exposure to the DB. The histological images obtained in this study were consistent with those obtained in a previous study that reported that the thickness of the epithelial layer in RHG increased after exposure to a biofilm (Shang *et al.* 2018). The commensal DB contributes to the gingival epithelial tissue to maintain homeostasis as the barrier.

This study had a few limitations. First, the culture conditions for the DB and RHG differed from that of the oral cavity because saliva, which is the main nutrient source for DBs (Marsh *et al.* 2016), was not used for culturing DBs to prevent changes in the microbiome of the experimental DB induced by components of the saliva. Secondly, the comprehensive analyses on metabolites and gene expression, such as metabolome analysis and RNA sequencing, were not performed owing to high costs; instead, the metagenomic function prediction analysis was performed using PICRUSt2. Finally, the RHG model in this study did not contain immune cells, although oral diseases such as periodontitis are highly associated with host immune cells (Graves 2008, Abdulkareem *et al.* 2023). Future studies should establish new host gingival models that contain immune cells such as neutrophils. In the DB cocultured with RHG, Veillonella increased and it may impact the characteristic of RHG. Veillonella could have affected RHG; however, it is difficult to isolate Veillonella from the *in situ* DB and/or oral bacteria. Moreover, not only one bacterial species can impact RHG; multispecies bacteria may be associated with the interaction between the DB and the host (Redanz *et al.* 2021). The effects of Veillonella on RHG should be investigate as a further study.

In conclusion, we found that the microbiome and functions of DBs can be affected by host gingival tissues. This is the first study to investigate the changes in DBs cocultured with a host gingival model. Our findings will contribute to the establishment of a host–biofilm interaction model to understand the pathophysiology of oral infectious diseases, such as periodontitis.

Supplementary materials

This is linked to the online version of the paper at https://doi.org/10.1530/MAH-24-0008.

Declaration of interest

The authors declare that there is no conflict of interest that could be perceived as prejudicing the impartiality of the work.

Funding

This study was supported by JSPS KAKENHI Grant Numbers 21K16990, 20K23104 and 24K02763. A portion of this study was supported by the MSD Life Science Foundation.

Author contributions

MS performed conceptualization, analysis, funding acquisition, validation, investigation and visualization in this study and wrote the original draft. RT performed analysis and investigation. TI contributed to the methodology. RN, RS, NK and JM performed investigation. ST contributed to conceptualization, funding acquisition and methodology. YN performed supervision and writing, review and editing of the manuscript.

Data availability

The 16S rRNA sequencing data are available from BioProject under the Accession Number PRJDB18360.

References

Aagaard K, Petrosino J, Keitel W, *et al.* 2013 The Human Microbiome Project strategy for comprehensive sampling of the human microbiome and why it matters. *FASEB J* **27** 1012–1022. (https://doi.org/10.1096/fj.12-220806)

Aas JA, Paster BJ, Stokes LN, *et al.* 2005 Defining the normal bacterial flora of the oral cavity. *J Clin Microbiol* **43** 5721–5732. (https://doi.org/10.1128/jcm.43.11.5721-5732.2005)

Abdulkareem AA, Al-Taweel FB, Al-Sharqi AJB, *et al.* 2023 Current concepts in the pathogenesis of periodontitis: from symbiosis to dysbiosis. *J Oral Microbiol* **15** 2197779. (https://doi.org/10.1080/20002297.2023.2197779)

Asikainen S, Chen C & Slots J 1996 Likelihood of transmitting *Actinobacillus actinomycetemcomitans* and *Porphyromonas gingivalis* in families with periodontitis. *Oral Microbiol Immunol* **11** 387–394. (https://doi.org/10.1111/j.1399-302x.1996.tb00200.x)

Baldeon-Gutierrez R, Ohkura N, Yoshiba K, *et al.* 2024 Wound-healing processes after pulpotomy in the pulp tissue of type 1 diabetes mellitus model rats. *J Endod* **50** 196–204. (https://doi.org/10.1016/j.joen.2023.10.016)

Bals R, Wang X, Wu Z, *et al.* 1998 Human beta-defensin 2 is a salt-sensitive peptide antibiotic expressed in human lung. *J Clin Invest* **102** 874–880. (https://doi.org/10.1172/jci2410)

Bogefors J, Kvarnhammar AM, Hockerfelt U, *et al.* 2012 Reduced tonsillar expression of human β-defensin 1, 2 and 3 in allergic rhinitis. *FEMS Immunol Med Microbiol* **65** 431–438. (https://doi.org/10.1111/j.1574-695x.2012.00959.x)

Brestoff JR & Artis D 2013 Commensal bacteria at the interface of host metabolism and the immune system. *Nat Immunol* **14** 676–684. (https://doi.org/10.1038/ni.2640)

Brown JL, Johnston W, Delaney C, *et al.* 2019 Biofilm-stimulated epithelium modulates the inflammatory responses in co-cultured immune cells. *Sci Rep* **9** 15779. (https://doi.org/10.1038/s41598-019-52115-7)

Buskermolen JK, Reijnders CM, Spiekstra SW, *et al.* 2016 Development of a full-thickness human gingiva equivalent constructed from immortalized keratinocytes and fibroblasts. *Tissue Eng Part C Methods* **22** 781s–791. (https://doi.org/10.1089/ten.tec.2016.0066)

Chandra A, Srivastava RK, Kashyap MP, *et al.* 2011 The anti-inflammatory and antibacterial basis of human omental defense: selective expression of cytokines and antimicrobial peptides. *PLoS One* **6** e20446. (https://doi.org/10.1371/journal.pone.0020446)

Clarke JK 1924 On the bacterial factor in the etiology of dental caries. *Br J Exp Pathol* **5** 141–147.

Filho GS, Caballé-Serrano J, Sawada K, *et al.* 2015 Conditioned medium of demineralized freeze-dried bone activates gene expression in periodontal fibroblasts in vitro. *J Periodontol* **86** 827–834. (https://doi.org/10.1902/jop.2015.140676)

Graves D 2008 Cytokines that promote periodontal tissue destruction. *J Periodontol* **79** 1585–1591. (https://doi.org/10.1902/jop.2008.080183)

Hajishengallis G & Lamont RJ 2012 Beyond the red complex and into more complexity: the polymicrobial synergy and dysbiosis (PSD) model of periodontal disease etiology. *Mol Oral Microbiol* **27** 409–419. (https://doi.org/10.1111/j.2041-1014.2012.00663.x)

Hall MW, Singh N, Ng KF, *et al.* 2017 Inter-personal diversity and temporal dynamics of dental, tongue, and salivary microbiota in the healthy oral cavity. *NPJ Biofilms Microbiomes* **3** 2. (https://doi.org/10.1038/s41522-016-0011-0)

Harder J, Bartels J, Christophers E, *et al.* 2001 Isolation and characterization of human μ-defensin-3, a novel human inducible peptide antibiotic. *J Biol Chem* **276** 5707–5713. (https://doi.org/10.1074/jbc.m008557200)

Harder J, Meyer-Hoffert U, Teran LM, *et al.* 2000 Mucoid *Pseudomonas aeruginosa*, TNF-α, and IL-1 β, but not IL-6, induce human β-defensin-2 in respiratory epithelia. *Am J Respir Cell Mol Biol* **22** 714–721. (https://doi.org/10.1165/ajrcmb.22.6.4023)

Holm CK & Qu C 2022 Engineering a 3D in vitro model of human gingival tissue equivalent with genipin/cytochalasin D. *Int J Mol Sci* **23** 7401. (https://doi.org/10.3390/ijms23137401)

The Human Microbiome Project Consortium 2012*a* A framework for human microbiome research. *Nature* **486** 215–221. (https://doi.org/10.1038/nature11209)

The Human Microbiome Project Consortium 2012*b* Structure, function and diversity of the healthy human microbiome. *Nature* **486** 207–214. (https://doi.org/10.1038/nature11234)

Kinane DF, Stathopoulou PG & Papapanou PN 2017 Periodontal diseases. *Nat Rev Dis Primers* **3** 17038. (https://doi.org/10.1038/nrdp.2017.38)

Kroes I, Lepp PW & Relman DA 1999 Bacterial diversity within the human subgingival crevice. *Proc Natl Acad Sci U S A* **96** 14547–14552. (https://doi.org/10.1073/pnas.96.25.14547)

L'Heureux JE, van der Giezen M, Winyard PG, *et al.* 2023 Localisation of nitrate-reducing and highly abundant microbial communities in the oral cavity. *PLoS One* **18** e0295058. (https://doi.org/10.1371/journal.pone.0295058)

Liou MJ, Miller BM, Litvak Y, *et al.* 2022 Host cells subdivide nutrient niches into discrete biogeographical microhabitats for gut microbes. *Cell Host Microbe* **30** 836–847.e6. (https://doi.org/10.1016/j.chom.2022.04.012)

Lundberg JO, Gladwin MT, Ahluwalia A, *et al.* 2009 Nitrate and nitrite in biology, nutrition and therapeutics. *Nat Chem Biol* **5** 865–869. (https://doi.org/10.1038/nchembio.260)

Marsh PD, Do T, Beighton D, *et al.* 2016 Influence of saliva on the oral microbiota. *Periodontology 2000* **70** 80–92. (https://doi.org/10.1111/prd.12098)

Pahumunto N, Chotjumlong P, Makeudom A, *et al.* 2017 Pro-inflammatory cytokine responses in human gingival epithelial cells after stimulation with cell wall extract of Aggregatibacter actinomycetemcomitans subtypes. *Anaerobe* **48** 103–109. (https://doi.org/10.1016/j.anaerobe.2017.08.001)

Peres MA, Macpherson LMD, Weyant RJ, *et al.* 2019 Oral diseases: a global public health challenge. *Lancet* **394** 249–260. (https://doi.org/10.1016/s0140-6736(19)31146-8)

Periasamy S & Kolenbrander PE 2009 Mutualistic biofilm communities develop with Porphyromonas gingivalis and initial, early, and late colonizers of enamel. *J Bacteriol* **191** 6804–6811. (https://doi.org/10.1128/jb.01006-09)

Periasamy S & Kolenbrander PE 2010 Central role of the early colonizer Veillonella sp. in establishing multispecies biofilm communities with initial, middle, and late colonizers of enamel. *J Bacteriol* **192** 2965–2972. (https://doi.org/10.1128/jb.01631-09)

Prado-Montes de Oca E 2010 Human beta-defensin 1: a restless warrior against allergies, infections and cancer. *Int J Biochem Cell Biol* **42** 800–804. (https://doi.org/10.1016/j.biocel.2010.01.021)

Redanz U, Redanz S, Treerat P, *et al.* 2021 Differential response of oral mucosal and gingival cells to *Corynebacterium durum, Streptococcus sanguinis*, and *Porphyromonas gingivalis* multispecies biofilms. *Front Cell Infect Microbiol* **11** 686479. (https://doi.org/10.3389/fcimb.2021.686479)

Shang L, Deng D, Buskermolen JK, *et al.* 2018 Multi-species oral biofilm promotes reconstructed human gingiva epithelial barrier function. *Sci Rep* **8** 16061. (https://doi.org/10.1038/s41598-018-34390-y)

Simón-Soro A & Mira A 2015 Solving the etiology of dental caries. *Trends Microbiol* **23** 76–82. (https://doi.org/10.1016/j.tim.2014.10.010)

Simon-Soro A, Ren Z, Krom BP, *et al.* 2022 Polymicrobial aggregates in human saliva build the oral biofilm. *mBio* **13** e0013122. (https://doi.org/10.1128/mbio.00131-22)

Sotozono M, Kuriki N, Asahi Y, *et al.* 2021*a* Impact of sleep on the microbiome of oral biofilms. *PLoS One* **16** e0259850. (https://doi.org/10.1371/journal.pone.0259850)

Sotozono M, Kuriki N, Asahi Y, *et al.* 2021*b* Impacts of sleep on the characteristics of dental biofilm. *Sci Rep* **11** 138. (https://doi.org/10.1038/s41598-020-80541-5)

Suzuki MT & Giovannoni SJ 1996 Bias caused by template annealing in the amplification of mixtures of 16S rRNA genes by PCR. *Appl Environ Microbiol* **62** 625–630. (https://doi.org/10.1128/aem.62.2.625-630.1996)

Wake N, Asahi Y, Noiri Y, *et al.* 2016 Temporal dynamics of bacterial microbiota in the human oral cavity determined using an *in situ* model of dental biofilms. *NPJ Biofilms Microbiomes* **2** 16018. (https://doi.org/10.1038/npjbiofilms.2016.18)

Weisburg WG, Barns SM, Pelletier DA, *et al.* 1991 16S ribosomal DNA amplification for phylogenetic study. *J Bacteriol* **173** 697–703. (https://doi.org/10.1128/jb.173.2.697-703.1991)

Wolgin M, Liodakis S, Ulrich I, *et al.* 2012 Gene expression of human beta defensins-1 and -2 is significantly reduced in non-inflamed keratinized oral tissue of smokers. *J Dent* **40** 949–954. (https://doi.org/10.1016/j.jdent.2012.07.017)

Yao S, Hao L, Zhou R, *et al.* 2022 Formation of biofilm by *Tetragenococcus halophilus* benefited stress tolerance and anti-biofilm activity against *S. aureus* and *S. Typhimurium*. *Front Microbiol* **13** 819302. (https://doi.org/10.3389/fmicb.2022.819302)

Zhang D, Xu T, Xu Q, *et al.* 2021 Expression profile of macrophage migration inhibitory factor in periodontitis. *Arch Oral Biol* **122** 105003. (https://doi.org/10.1016/j.archoralbio.2020.105003)